Thermal and electronic properties of $CePd_3In_2$

H. Kaldarar,[1] E. Royanian,[1] H. Michor,[1] G. Hilscher,[1] E. Bauer,[1] A. Gribanov,[2,3] D. Shtepa,[2] P. Rogl,[3] A. Grytsiv,[3] Y. Seropegin,[2] and S. Nesterenko[2]

[1]*Institute of Solid State Physics, Vienna University of Technology, Wien A-1040, Austria*

[2]*Department of Chemistry, Moscow State University, Leninskie Gory, GSP-1, Moscow 119991, Russia*

[3]*Institute of Physical Chemistry, University of Vienna, Währingerstrasse 42, Wien A-1090, Austria*

(Received 13 November 2008; published 7 May 2009)

In this work, we report on the physical properties of orthorhombic $CePd_3In_2$ in comparison with isotypic $LaPd_3In_2$ (space group *Pnma*). X-ray powder diffraction Rietveld analysis revealed single-phase composition of both specimens $CePd_3In_2$ and $LaPd_3In_2$ confirming the $CePd_3In_2$ type with space group *Pnma*. The lattice parameters are $a=1.02788(8)$, $b=0.46237(4)$, and $c=0.98765(9)$ nm for $CePd_3In_2$ and $a=1.02986(14)$, $b=0.46424(6)$, and $c=0.99498(13)$ nm for $LaPd_3In_2$. Physical properties of $CePd_3In_2$ at low temperatures are dominated by a magnetic phase transition into an antiferromagnetic ground state below $T_N \sim 2.1$ K. A mutual interplay of the Kondo effect and the Rudermann-Kittel-Kasuy-Yoshida interaction is responsible for a large Sommerfeld value $\gamma \sim 500$ mJ/mol K^2 derived from a model which simultaneously describes the Kondo effect and long-range magnetic order.

DOI: 10.1103/PhysRevB.79.205104 PACS number(s): 75.30.Mb, 75.40.Cx, 75.50.Ee

I. INTRODUCTION

Many cerium-based intermetallics exhibit interesting physics such as superconductivity, valence fluctuations, heavy fermion behavior, and non-Fermi-liquid features. These properties result, in general, from a competition between the Rudermann-Kittel-Kasuy-Yoshida (RKKY) interaction and the Kondo effect. Such a balance of interactions takes place in an environment defined from the lifting of the sixfold degenerate ground state of the Ce $j=5/2$ total angular momentum owing to crystalline electric field (CEF) effects.[1] Earlier, two compounds from the ternary system Ce-Pd-In, i.e., Ce_2Pd_2In and CePdIn, were investigated in detail.[2–4] While the former shows either ferromagnetic or an antiferromagnetic ordering, depending on slight off-stoichiometry of the system, the latter undergoes antiferromagnetic order at $T_N=1.65$ K. Within Doniach's phase diagram, CePdIn is close to a quantum critical point[4] due to the Kondo effect, tending to prevent long-range magnetic order established by the RKKY interaction. The crystal structure of the compound $CePd_3In_2$, first reported by Giovannini *et al.* in Ref. 5, was derived from single crystal x-ray data as a new orthorhombic structure type with space group *Pnma*.[6] As, hitherto no physical properties of this compound were published in literature, the present work aims to characterize the ground-state properties of $CePd_3In_2$, in comparison with the new isotypic nonmagnetic compound $LaPd_3In_2$, defining the lattice dynamics of the materials.

II. EXPERIMENT

Polycrystalline samples of $CePd_3In_2$ and $LaPd_3In_2$ were prepared from high-purity metal ingots by a standard arc melting procedure on a water-cooled copper hearth under an argon atmosphere with zirconium getter followed by annealing at 900 °C during 240 h. The specimens were remelted three times to ensure complete fusion. The mass losses after arc melting were less than 1 mass %. X-ray powder diffraction intensity data were collected on an Guinier Huber image plate 670 (Cu $K_{\alpha 1}$ radiation) and were treated with the FULLPROF program.[7,8] Precise lattice parameters were calibrated against Ge as internal standard ($a_{Ge}=0.565\,754$ nm) (Ref. 9) using program STOE-WINXPOW.[10] Physical bulk properties were determined using a number of standard techniques as described, e.g., in Ref. 11.

III. RESULTS AND DISCUSSION

Rietveld analyses of the x-ray diffraction data of $CePd_3In_2$ and $LaPd_3In_2$ confirmed in both cases the structure model with full atom order as derived earlier for $CePd_3In_2$ (Ref. 6) (see Fig. 1). X-ray diffraction data are listed in Table I. Rietveld refinements show (Figs. 2 and 3) that both samples were single phase.

Figure 4(a) shows the temperature-dependent magnetic susceptibility χ plotted as $1/\chi$ vs T for $CePd_3In_2$ from 2 to 300 K. The almost linear temperature dependence of $1/\chi$ above about 50 K refers to a Ce $4f^1$ magnetic configuration

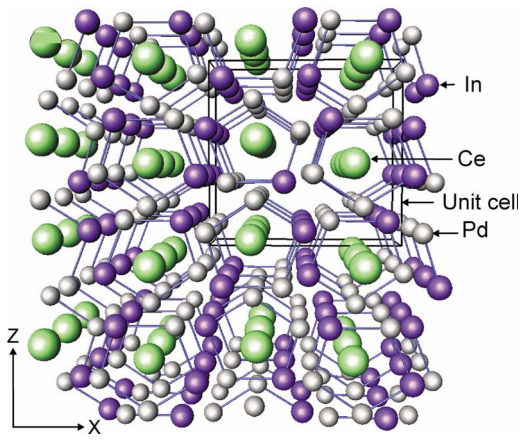

FIG. 1. (Color online) Perspective view of the $CePd_3In_2$ crystal structure along the Y axis.

TABLE I. Crystallographic data for $CePd_3In_2$ and $LaPd_3In_2$; Rietveld analyses (x-ray data at RT from image plate, Cu $K_{\alpha 1}$ radiation), space group *Pnma*; crystal structure model was taken from Ref. 6.

	Lattice parameters (nm)			
Compound	*a*	*b*	*c*	$R_F=\Sigma\|F_o-F_c\|/\Sigma F_o$
$CePd_3In_2$	1.02788(8)	0.46237(4)	0.98765(9)	0.054
$LaPd_3In_2$	1.02986(14)	0.46424(6)	0.99498(13)	0.042

of the Ce ions. To quantitatively account for this region, a least-squares fit according to the modified Curie Weiss law, i.e., $\chi=\chi_0+C/(T-\theta_p)$ was applied. $\chi_0=3.10^{-4}$ emu/mol represents a temperature-independent Pauli-type susceptibility, C is the Curie constant yielding an effective moment $\mu_{\text{eff}}=2.43\mu_B$, and $\theta_p=-8$ K is the paramagnetic Curie temperature. The effective magnetic moment is close to the theoretical value associated with the Ce^{3+} state, i.e., $2.54\mu_B$, corroborating the $4f^1$ electronic configuration of the Ce ions.

The slight curvature of the inverse magnetic susceptibility observed below 50 K is attributed to CEF effects. A substantial density of states at the Fermi energy is obvious from a relatively large Pauli-type susceptibility and is associated with the 3*d* band of the Pd sublattice. This is in accordance with the finding that $LaPd_3In_2$ is Pauli paramagnetic with a temperature-independent susceptibility of about 5.10^{-4} emu/mol (see inset of Fig. 4 for comparison). The slightly larger Pauli susceptibility of $LaPd_3In_2$ than that of $CePd_3In_2$ (3.10^{-4} emu/mol) derived from the modified Curie Weiss fit might be attributed to tiny magnetic impurities giving rise to a rather small low-temperature upturn, which, however, is not visible on that scale in Fig. 4(b). Additionally, the Pauli susceptibility can be related to the electronic specific-heat contribution in $LaPd_3In_2$ with a Sommerfeld constant of about $\gamma=7$ mJ/mol K^2 (see below) yielding a density of states at the Fermi energy $N(E_F)=1.5$ states/(eV spin f.u.). In order to obtain good agreement for $N(E_F)$ from both the susceptibility and specific heat data, we have to assume a Stoner enhancement factor of about 5–8, where we also included a correction for the core diamagnetism. In general, a Stoner enhancement factor of about 5–10 is a typical quantity for Pd compounds.

The negative paramagnetic Curie temperature refers to antiferromagnetic interactions between the almost localized Ce 4*f* moments and the conduction electrons. In terms of the Kondo effect, usually present in cerium compounds, the characteristic temperature scale, i.e., the Kondo temperature can be estimated from $T_K\sim|\theta_p/4|$ suggesting $T_K\sim 2$ K.[12] Figure 4(b) displays low-temperature susceptibility data taken at 0.1, 1, 3, and 5 T, respectively. Clearly visible is the anomaly in the low-field data at $T\sim 2.2$ K, indicating the onset of long-range magnetic order, corroborated by resistivity and heat-capacity data (see below). The shift of the $\chi(T)$ peak to lower temperatures with increasing magnetic fields is synonymous to an antiferromagnetic ground state. Electrical resistivity measurements allow deep insight into electronic, magnetic, and thermal properties of materials, revealing conclusions about magnetic phase transition temperatures, types of interactions or about metallic or insulating ground states.

Shown in Fig. 5 is the temperature-dependent electrical resistivity ρ of $CePd_3In_2$ from 400 mK to room temperature plotted on a logarithmic temperature axis. For the purpose of comparison, $\rho(T)$ of isomorphous nonmagnetic $LaPd_3In_2$ is added. The latter serves to define the lattice dynamics of the compounds. $LaPd_3In_2$ behaves metallic in the whole temperature range investigated and can be accounted for in terms of the modified Bloch-Grüneisen formula, where a T^3 term

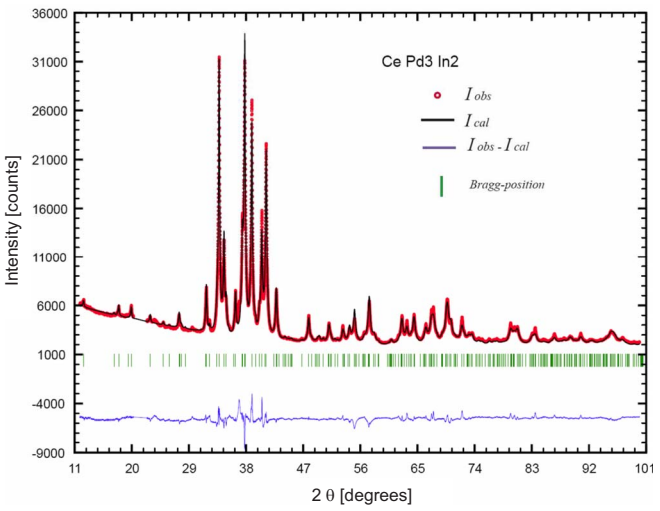

FIG. 2. (Color online) Rietveld refinement of powder x-ray diffraction pattern of $CePd_3In_2$.

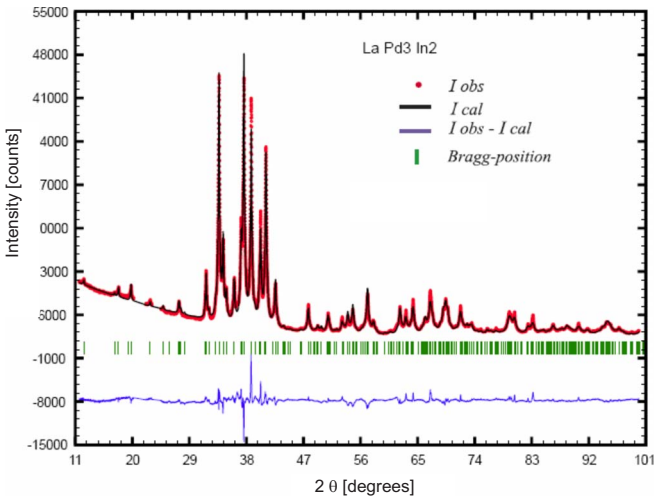

FIG. 3. (Color online) Rietveld refinement of powder x-ray diffraction pattern of $LaPd_3In_2$.

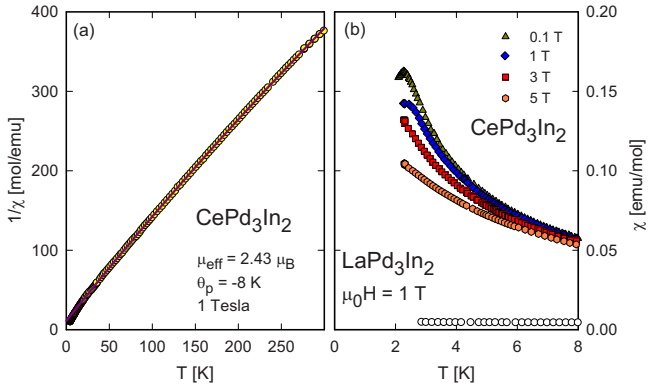

FIG. 4. (Color online) (a) Temperature-dependent magnetic susceptibility χ of $CePd_3In_2$ plotted as $1/\chi$ vs T. Data are taken at $\mu_0 H = 1$ T. The solid line is a least-square fit according to the modified Curie Weiss law. (b) Low-temperature susceptibility of $CePd_3In_2$ taken at various externally applied magnetic fields. $LaPd_3In_2$ is added for a purpose of comparison.

(Mott-Jones term) is added in order to account for a narrow electronic structure near to the Fermi energy which is expected to be originated from the Pd $4d$ band. Results of a least-squares fit are shown in Fig. 5 as solid line, revealing the Debye temperature $\theta_{D,\rho} = 145$ K and excellent agreement with the experimental data. An equally good fit is observed if the well-known parallel resistor formula is applied,[13] where the ideal resistance is represented by the standard Bloch-Grüneisen law and the saturation resistivity being as large as 696 $\mu\Omega$ cm. In this case, the Debye temperature is slightly larger about 150 K. The low value of the residual resistivity (8.5 $\mu\Omega$ cm) refers to a good metal and a well-ordered crystal structure, where site interchanges of La, Pd, and In are almost excluded.

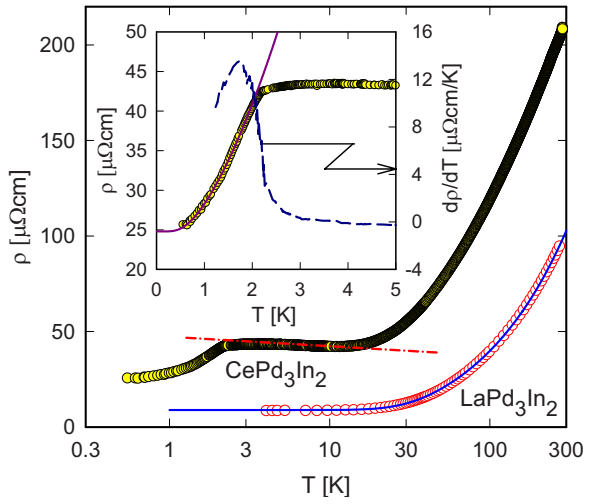

FIG. 5. (Color online) Temperature-dependent electrical resistivity ρ of $CePd_3In_2$ and $LaPd_3In_2$. The solid line is a least-squares fit to the $LaPd_3In_2$ data (see the text) and the dashed-dotted line guides the eyes. The inset shows low-temperature details of $\rho(T)$ of $CePd_3In_2$ with the magnetic phase-transition temperature $T_N \sim 2$ K. The solid line is a least-squares fit and the dashed line (referring to the right axis) reveals $d\rho/dT$, clearly evidencing the magnetic phase transition.

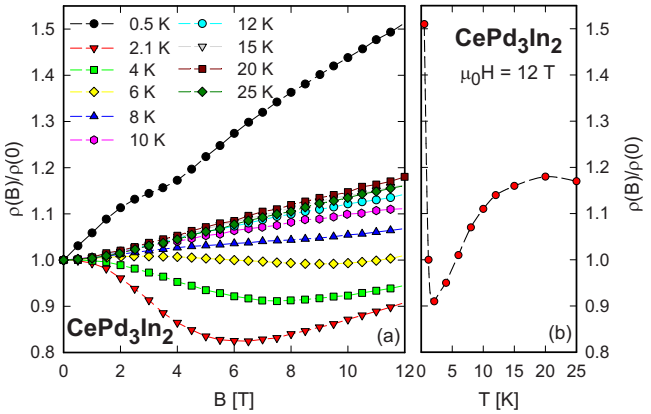

FIG. 6. (Color online) (a) Isothermal magnetoresistance $\rho(B)/\rho(0)$ of $CePd_3In_2$ for various temperatures. (b) Temperature-dependent magnetoresistance of $CePd_3In_2$ taken at $\mu_0 H = 12$ T.

A distinctly different behavior of $\rho(T)$ is observed for $CePd_3In_2$. Two easily accessible features are obvious: (i) a negative logarithmic dependence of $\rho(T)$ below about 20 K, following by (ii) a drop of the resistivity below about 2 K. While the former refers to Kondo-type interaction, the latter evidences a magnetic phase transition (seen in more detail in the inset of Fig. 5). The smooth change of $\rho(T)$ from the paramagnetic to the magnetically ordered state implies a second-order phase transition. In order to qualitatively account for the ordered region of $CePd_3In_2$, a model developed in Ref. 14 is applied, yielding an analytic expression regarding the temperature-dependent electrical resistivity,

$$\rho = \rho_0 + A\Delta^{3/2}T^{1/2}\exp\left(-\frac{\Delta}{T}\right)\left[1 + \frac{2}{3}\left(\frac{T}{\Delta}\right) + \frac{2}{15}\left(\frac{T}{\Delta}\right)^2\right]. \quad (1)$$

This expression is based on scattering of conduction electrons on antiferromagnetic magnons with a dispersion relation given by $\omega = \sqrt{\Delta^2 + D^2k^2}$, where Δ is the spin-wave gap and D is the spin wave velocity; $A \propto 1/D^3 \propto \Gamma^3$; Γ is an effective coupling between the Ce ions. Applying Eq. (1) to the experimental data yields a spin-wave gap $\Delta = 1.5$ K, reasonable with respect to the magnetic phase-transition temperature of about 2 K. Results of this fit are shown as solid line in the inset of Fig. 5. A derivative $d\rho/dT$ (inset of Fig. 5, right axis) of the experimental data at low temperatures clearly marks the magnetic phase transition.[15]

The magnetoresistance $\rho(B)/\rho(0)$ is plotted in Fig. 6(a) as a function of the externally applied magnetic field. $\rho(B)/\rho(0)$ shows a nonmonotonous behavior [compare the values at 12 T in Fig. 6(b)]. Within the magnetically ordered-state large positive values are found, exhibiting a weak anomaly around 4 T, which may result from a field driven reorientation of the magnetic structure. These $\rho(B)/\rho(0)$ data also indicate that these reorientation might not be a field-driven ferromagnetic state since in such a case, a reduction in $\rho(B)/\rho(0)$ is expected on a further increase in the magnetic field. The magnetoresistance becomes negative for a narrow temperature range above the magnetic phase-transition temperature due to the suppression of magnetic fluctuations associated with

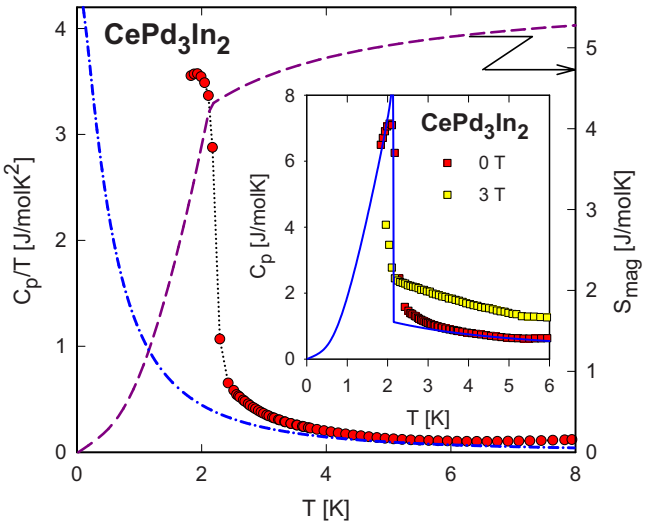

FIG. 7. (Color online) Temperature-dependent specific heat C_p of $CePd_3In_2$ plotted as C_p/T vs T and C_p vs T (inset). The dotted line connecting experimental points is a guide for the eyes. The dashed-dotted line represents a Kondo contribution with $T_K=1.5$ K. The dashed line defines the magnetic entropy S_{mag} and refers to the right axis. The solid line in the inset shows a least-squares fit to the data as explained in the text. The inset also shows $C_p(T)$ for a measurement at 3 T.

the Kondo effect. Even for that range, a slight upturn at higher magnetic fields can be observed which may be attributed to the presence of a large and positive classical magnetoresistance, dominating the system above about 10 K. The decrease in the contribution originating from the Kondo effect results in an increase in the whole measured effect, although also the classical magnetoresistance decreases as the temperature increases. This becomes obvious above about 20 K, where $\rho(B)/\rho(0)$ starts to decrease. There are no procedures available in literature to separate the nonclassical magnetoresistance from the total measured effect, allowing to analyze the part stemming from the interaction of the conduction electrons with the Ce magnetic moments.

Long-range magnetic order is also corroborated from temperature-dependent heat-capacity measurements. Results are shown in Fig. 7. The sharp anomaly at 2.1 K refers to the onset of long-range magnetic order, in excellent agreement with the resistivity and susceptibility data. The application of an external magnetic field shifts the phase transition to lower temperatures, clearly evidencing antiferromagnetic order as magnetic ground state. The height of the specific-heat anomaly δ at $T=T_N$ is well below that associated with ordering within an unperturbed crystal field doublet as ground state ($\delta=12.5$ J/mol K). In general, such a reduction is attributed to the short-range order effects and/or Kondo-type interaction. The latter tends to screen the Ce $4f$ moments; as a result, both the ordering temperature and the magnetic entropy released at the phase transition are diminished.

Considering the Kondo effect as the primary cause of the observed reduced magnitude of the specific-heat anomaly, the resonant level model of Schotte and Schotte[16] can be used, and long-range magnetic order is incorporated in terms of the molecular-field theory.[17–19] The temperature-dependent specific heat can be evaluated from the spontaneous magnetization $M(T)$ of an effective $j=1/2$ system, revealing an analytical expression for the heat capacity[18]

$$C_{\mathrm{mag}} = 2k_B\Re\left(\frac{z}{T}\left[1-\left(\frac{z}{T}-\frac{\partial z}{\partial T}\right)\psi'\left(\frac{1}{2}+\frac{z}{T}\right)\right]\right), \qquad (2)$$

$z=[k_BT_K+iE(T)]/2\pi k_B$, ψ' is the digamma function, and E follows in the mean field theory from $E=g\mu_BB_0=g\mu\lambda M=J(M/M_0)$. B_0 refers to the molecular field, λ is the molecular field constant, J is the s-f coupling constant, and M_0 is the spontaneous magnetization at $T=0$. The best agreement between the experimental results and the predictions of Eq. (2) is revealed when taking $J=6$ K and $T_K=1.5$ K (solid line, inset of Fig. 7). Representing these model data as C_{mag}/T for $T\to 0$ directly defines the Sommerfeld value $\gamma\sim 500$ mJ/mol K^2. Note that a vanishing Kondo interaction, i.e., $k_BT_K=0$, will drive γ toward zero, leaving an unperturbed magnetically ordered ground state. Under these circumstances, the deduced s-f coupling constant $J=6$ K would lead to magnetic ordering at $T_N^0=3$ K, equivalent to $T_N=J/2$. Here, it should be noted that the simultaneous presence of the s-f coupling J and the Kondo effect reverses the well-known relation $T_K\sim 1/\gamma$. Rather, keeping the s-f coupling constant while increasing the Kondo interaction strength causes γ to rise within a limited range of the ratio J/T_K.

Of course, this phenomenological model [Eq. (2)] is unable to account for short-range ordering effects, responsible for the observed broadening of the magnetic phase transition (compare the differences in the inset of Fig. 7). On the other hand, if Kondo interactions alone would determine the ground-state properties, the Sommerfeld value $\gamma=C_p/T(T\to 0)$ would reach enormously large values (dashed-dotted line, Fig. 7). A further signature of the presence of the Kondo effect may be drawn from the reduced entropy derived at $T=T_N$. While unperturbed magnetic ordering within a CEF ground-state doublet releases an entropy of R ln 2, the observed value (4.3 J/mol K) is reduced by more than 20%, indicating a weak Kondo effect. The fact that R ln 2 is not reached below 10 K is equivalent to a CEF level scheme, where the first- and the second-excited levels are energetically well separated from the ground state.

In order to obtain more information about the CEF splitting, the difference of the specific-heat data of magnetic $CePd_3In_2$ and nonmagnetic $LaPd_3In_2$ is shown in Fig. 8 plotted as $\Delta C_p(T)$ (right axis), together with the measured heat capacities. Applying the standard model analysis to $C_p(T)$ of $LaPd_3In_2$, i.e., $C_p(T)=\gamma T+\beta T^3$ to temperatures below 6 K reveals the Sommerfeld constant $\gamma=6$ mJ/mol K^2 and $\theta_{D,LT}=220$ K. In order to account for the entire temperature range of $C_p(T)$ of $LaPd_3In_2$, the Debye model with $\theta_D=205$ K, and at least three Einstein frequencies with 44, 100, and 210 K and relative weights of 1, 5, and 9, respectively, (dashed line of Fig. 8) have to be taken into consideration. This model allows for three acoustic and 15 optical phonon modes, evidencing a rather complicated phonon spectrum. The magnetic contribution $C_{\mathrm{mag}}\sim\Delta C_p$ at elevated temperatures shows a typical Schottky anomaly, and a fit of

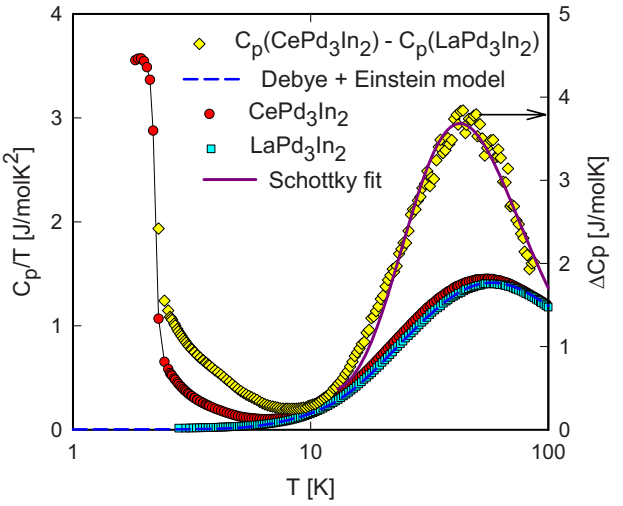

FIG. 8. (Color online) Temperature-dependent specific heat C_p of $CePd_3In_2$ and $LaPd_3In_2$ plotted as C_p/T vs T. The difference data set refers to the right axis and is plotted as ΔC_p vs T. The solid line is a least-squares fit as explained in the text and the dashed line represents the Debye model together with three Einstein frequencies.

the data reveals the first-excited doublet above the ground-state doublet at $\Delta_1 \sim 105$ K (solid line in Fig. 8), in good agreement with the conclusion drawn from the entropy data. The uppermost level of this system lies well above room temperature, thus does not influence the data of the temperature range studied.

IV. SUMMARY

A variety of bulk properties studied in a temperature range from 400 mK to room temperature characterizes $CePd_3In_2$ as an antiferromagnetically ordered system (T_N=2.1 K) in the presence of a weak Kondo effect. Magnetic order occurs in a doublet as ground state coming from CEF splitting of the $j=5/2$ total angular momentum of the Ce ion in orthorhombic symmetry. The first- and the second-excited CEF levels appear to be well separated from the ground state, thus do not significantly contribute to the magnetic order and Kondo effect ($\Delta_{CEF} \gg T_N, T_K$). Both $LaPd_3In_2$ and $CePd_3In_2$ behave metallic and the phonon spectrum of these ternary compounds may be accounted for in terms of a Debye model modified by a few Einstein branches. The fairly low Debye temperature characterizes these systems as rather soft. This might result from the presence of rather heavy elements constituting these materials. The low-residual resistivity of $LaPd_3In_2$ evidences that the crystal structure is regular and intersite atom exchange of Pd and In is small.

ACKNOWLEDGMENTS

The authors are grateful to RFBR under Projects No. 06-03-90579_BNTS and No. 08-03-01072 and to the Austrian-Russian bilateral exchange program OEAD under Project No. I.17/2006, as well as to the Austrian FWF under Project No. P18054.

[1] J. G. Sereni, in *Handbook for Physics and Chemistry of Rare Earths*, edited by K. A. Gschneidner, Jr. and L. Eyring (Elsevier Science B. V, New York, 1991), Vol. 15, Chap. 98.
[2] M. Giovannini, H. Michor, E. Bauer, G. Hilscher, P. Rogl, T. Bonelli, F. Fauth, P. Fischer, T. Herrmannsdörfer, L. Keller, W. Sikora, A. Saccone, and R. Ferro, Phys. Rev. B **61**, 4044 (2000).
[3] P. Fischer, T. Herrmannsdörfer, T. Bonelli, F. Fauth, L. Keller, E. Bauer, and M. Giovannini, J. Phys.: Condens. Matter **12**, 7089 (2000).
[4] B. Chevalier, A. Wattiaux and J.-L. Bobet, J. Phys.: Condens. Matter **18**, 1743 (2006).
[5] M. Giovannini, A. Saccone, P. Rogl, and R. Ferro, Intermetallics **11**, 197 (2003).
[6] S. N. Nesterenko, A. I. Tursina, P. Rogl, and Y. D. Seropegin, J. Alloys Compd. **373**, 220 (2004).
[7] J. Rodriguez-Carvajal, Physica B **192**, 55 (1992).
[8] T. Roisnel and J. Rodriguez-Carvajal, *WinPLOTR: a Windows tool for powder diffraction patterns analysis*, Materials Science Forum, Proceedings of the Seventh European Powder Diffraction Conference, edited by R. Delhez and E. J. Mittenmeijer (2000), pp. 118–123.
[9] J. Emsley, *The Elements* (Clarendon, Oxford, 1991).
[10] *WINXPOW: Version 1.06* (Stoe & Cie GmbH, Darmstadt, Germany, 1999).
[11] E. Bauer, St. Berger, Ch. Paul, M. Della Mea, G. Hilscher, H. Michor, M. Reissner, W. Steiner, A. Grytsiv, P. Rogl, and E. W. Scheidt, Phys. Rev. B **66**, 214421 (2002).
[12] *Hewson: The Kondo Problem to Heavy Fermions* (Cambridge University Press, Cambridge, 1993), p. 52.
[13] O. Gunnarsson, M. Calandra, and J. E. Han, Rev. Mod. Phys. **75**, 1085 (2003).
[14] A. Continentino, S. N. de Medeiros, M. T. D. Orlando, M. B. Fontes, and E. M. Baggio-Saitovitch, Phys. Rev. B **64**, 012404 (2001).
[15] M. E. Fisher and J. S. Langer, Phys. Rev. Lett. **20**, 665 (1968).
[16] K. D. Schotte and U. Schotte, Phys. Lett. A **55**, 38 (1975).
[17] C. D. Bredl, F. Steglich, and K. D. Schotte, Z. Phys. B **29**, 327 (1978).
[18] A. Braghta, Ph.D. thesis, University of Strasbourg, 1989.
[19] M. J. Besnus and A. Braghta, N. Hamdaoui, and A. Meyer, J. Magn. Magn. Mater. **104-107**, 1385 (1992).